Assessing the Capacity Value of Energy Storage that Provides Frequency Regulation

Hyeong Jun Kim, *Student Member, IEEE,* Ramteen Sioshansi, *Fellow, IEEE,*
Eamonn Lannoye, *Senior Member, IEEE,* and Erik Ela, *Senior Member, IEEE*

***Abstract*—Due to complexity in determining its state of energy (SOE), multi-use applications complicate the assessment of energy storage's resource-adequacy contribution. SOE impacts resource-adequacy assessment because energy storage must have stored energy available to mitigate a loss of load. This paper develops a three-step process to assess the resource-adequacy contribution of energy storage that provides frequency regulation. First, we use discretized stochastic dynamic optimization to derive decision policies that tradeoff between different energy-storage applications. Next, the decision policies are used in a mixed-integer linear optimization that determines actual energy-storage operation in a rolling-horizon fashion. Finally, simulation is used to assess energy storage's resource-adequacy contribution. The methodology is demonstrated using a simple example and a case study that are based on actual real-world system data. We benchmark our proposed model to another that neglects frequency regulation and show the impacts of market design, frequency-regulation provision, and energy-storage size on the capacity value of energy storage.**

***Index Terms*—Power system security and risk analysis, ancillary service, capacity value, reliability theory, dynamic programming, energy storage**

I. Introduction

ENERGY storage is used increasingly for multiple applications [1]–[3], which can yield synergies and opportunity costs [4], [5]. Synergies arise if multiple applications call for the same operational profile (*e.g.*, discharging stored energy to exploit a high price can have a capacity-deferral benefit). Opportunity costs arise from conflicting applications (*e.g.*, discharging energy to exploit a high price may leave less energy to alleviate subsequent loss of load).

Opportunity costs between multiple services can complicate energy-storage assessment. Of particular importance is determining the contribution of energy storage towards the resource-adequacy needs of the electricity system in which it is located. This importance arises from planners needing to determine, potentially with a long lead time, that its electricity system can serve load reliably [6], [7]. There is a growing recognition that energy storage may play an outsize role in meeting the resource-adequacy needs of decarbonized electricity systems [8], [9]. Energy storage meeting resource-adequacy needs is tied to its state of energy (SOE). This relationship arises because energy storage must have stored energy available to mitigate a loss of load [10]–[13].

Thus, assessing energy storage's resource-adequacy contribution requires understanding how its SOE evolves. Its SOE depends on how energy storage is operated and exogenous factors. For instance, scheduling charging and discharging impacts energy-storage SOE. In addition, providing ancillary services may yield an uncertain energy-storage SOE (*e.g.*, due to real-time ancillary-service deployments).

Electricity-system reliability can be sensitive to operational decisions [14]. Its energy-limited nature can complicate such an assessment for energy storage. The technical literature tackles this challenge using analytic methods and simulation. Klöckl and Papaefthymiou [15] develop an approach that expresses energy-storage SOE as a function of its initial SOE and load, assuming that energy storage has unlimited energy capacity. Edwards *et al*. [12] use non-sequential simulation, assuming that energy storage can be charged fully overnight. Another approach [10], [13] uses dynamic optimization to compute an optimal decision policy, from which the probability distribution of SOE is derived. Examples of simulation-based works include that of Hu *et al*. [16], which considers different energy-storage-dispatch strategies. Koh *et al*. [17] compute reliability indices under different energy-storage-deployment scenarios. Zhou *et al*. [18] model the effective load carrying capability (ELCC) of energy storage that is used for peak-load shaving. Konstantelos *et al*. [19] use simulation to study the impact of network reliability on energy storage's ELCC.

A limitation of this literature is its focus on energy storage providing energy services (*e.g.*, energy shifting). Many energy-storage technologies are well suited to providing ancillary services (*e.g.*, frequency regulation) and energy storage is built for such applications [20]–[22]. Using energy storage for ancillary services can create opportunity costs *vis-à-vis* its resource-adequacy contribution. Providing high-value frequency regulation calls for maintaining 'headroom' to follow the real-time frequency-regulation signal [23]. Such headroom

Manuscript received 18 April, 2024; revised 16 August, 2024; accepted 9 November, 2024. This work was supported by National Science Foundation grants 1463492, 1808169, and 1922666, Electric Power Research Institute grants 00-10007617 and DKT230520, Carnegie Mellon Electricity Industry Center, and Wilton E. Scott Institute for Energy Innovation. *(Corresponding author: Hyeong Jun Kim.)*

H. J. Kim is with Department of Integrated Systems Engineering, The Ohio State University, Columbus, OH 43210-1271, USA (e-mail: kim.5206@buckeyemail.osu.edu).

R. Sioshansi is with Department of Engineering and Public Policy, Carnegie Mellon Electricity Industry Center, Department of Electrical and Computer Engineering, and Wilton E. Scott Institute for Energy Innovation, Carnegie Mellon University, Pittsburgh, PA 15213-3815, USA and with Department of Integrated Systems Engineering, The Ohio State University, Columbus, OH 43210-1271, USA (e-mail: rsioshan@andrew.cmu.edu).

E. Lannoye is with Grid Operations & Planning, EPRI Europe, Dublin, Ireland (elannoye@epri.com).

E. Ela is with Power Delivery and Utilization Department, Electric Power Research Institute, Palo Alto, CA 94304-1395, USA (e-mail: eela@epri.com).

conflicts with maintaining a high SOE to have stored energy available to alleviate a loss of load. In addition, a service such as frequency regulation introduces SOE uncertainty, because energy storage must charge and discharge to follow the frequency-regulation signal.

The literature includes works that model energy storage providing frequency regulation. One modeling approach employs linear optimization [24]–[26]. Unless it is used in a rolling-horizon fashion, linear optimization is static, insomuch as the modeled decisions might not be adjusted as new information is available. Dynamic optimization can overcome this limitation [4], [27], [28]. In addition to model structure, the analytical foci of these works differ. For instance, some works [24], [26], [29], [30] assess the revenues that energy storage can earn from providing energy and ancillary services whereas others [4], [27] develop models that could be used for real-time operation and trading-off between different applications.

This paper synthesizes these two streams of work to develop an approach to assess the resource-adequacy contribution of energy storage that provides frequency regulation. We begin in Section II by providing an exact model, which captures all of the pertinent dynamics and uncertainties, but is computationally intractable. Next, Section III provides our three-step approach, which is a tractable approximation of the exact model. First, stochastic dynamic optimization is used to derive decision policies. Next, optimal decision policies are used to build a mixed-integer linear optimization that determines, in a rolling-horizon fashion, real-time energy-storage operation. Finally, simulation is used to estimate energy storage's impact on electricity-system reliability. Section IV summarizes data generation and simulation, which are based on real-world data that correspond to an actual electricity system. Section V summarizes results for a one-day example and includes a comparison to a simpler exact model that neglects frequency regulation [13]. Section VI summarizes case-study results and Section VII concludes.

The novelty and primary contribution of our work is developing a resource-adequacy-assessment approach for energy storage that captures the SOE-related complexities of frequency regulation. Our work extends previous approaches to assessing the resource-adequacy contribution of energy storage [10], [13] by accounting for the provision of frequency regulation or other ancillary services. Our example and case study demonstrate the balance between computational tractability and model fidelity of our three-step approximation. Furthermore, we demonstrate the tradeoffs between the use of energy storage for resource adequacy and other applications. We explore also the effects of market-design and energy-storage-capacity choices on the resource-adequacy contribution of energy storage.

II. Exact Model

We model price-taking energy storage that provides energy shifting, frequency regulation, and capacity. Energy-shifting revenue is based on prices for charging and discharging energy. Without loss of generality, we model a single frequency-regulation product that includes upward and downward services. Some markets treat these as two separate products [31], [32], which can be captured by our model trivially. Energy storage receives a payment, based on a capacity price, for each MW of frequency-regulation capacity that it provides during a given hour. If energy storage is unable to follow the resultant frequency-regulation signal, it is penalized for its shortfall. We assume that energy storage has its rated capacity cleared in a capacity auction. We do not account for capacity-auction revenue, because it is a constant under our assumption. The capacity mechanism includes a non-performance penalty, which is levied against the energy storage if it is unable to operate at its rated capacity during a loss of load [33].

Our exact approach uses stochastic dynamic optimization to model energy-storage operations and to yield an optimal decision policy [34]. Our model can capture any uncertainty that impacts energy-storage operations or SOE. As detailed in Section IV, our example and case study consider uncertain prices, loss of load events, and frequency-regulation deployments. The policy that is obtained from the stochastic dynamic optimization is used to compute the probability distributions of the hourly energy-storage SOEs and to assess energy storage's resource-adequacy contribution.

A. Stochastic Dynamic Optimization

1) Stages: We consider an ordered set, T, of hours, each of which is a decision stage. t denotes the time index.

2) Decision Variables: For all $t \in T$, c_t and d_t denote scheduled hour-t energy-storage charging (MW) and discharging (MW), respectively, and n_t denotes hour-t frequency-regulation capacity (MW) that the energy storage schedules. For notational ease, $\forall t \in T$, we define:

$$a_t = (c_t, d_t, n_t)\,;$$

as a vector of hour-t decision variables.

3) State Variables: For all $t \in T$, there are four exogenous state variables. π_t and ρ_t are hour-t energy (\$/MWh) and frequency-regulation (\$/MW-h) prices, respectively. I_t is a binary variable that equals 0 if there is an hour-t loss of load and equals 1 otherwise. δ_t is the hour-$(t-1)$ dispatch-to-contract ratio (p.u.), which determines how much net energy must be charged or discharged by the energy storage to fulfill its frequency-regulation obligation [23], [35]. The one-hour offset in the index is due to the amount of energy that will be needed being unknown when the energy storage determines how much hour-t frequency regulation to schedule [4], [27]. There are two sets of endogenous state variables. For all $t \in T$, u_t is the amount of unfulfilled hour-$(t-1)$ frequency-regulation energy (MWh) and l_t is the beginning hour-t SOE of the energy storage (MWh). The same one-hour offset that is used to define δ_t is used in defining u_t. For all $t \in T$, we define:

$$W_t = (\pi_t, \rho_t, I_t, \delta_t, u_t)\,;$$

as a vector of hour-t state variables other than l_t.

4) State-Transition Functions: The exogenous state variables are simulated (*cf.* Sections II-C and IV). For all $t \in T$, the calculations of u_t and l_t depend on the sign of δ_t, because the sign determines whether the energy storage charges or discharges to fulfill its hour-$(t-1)$ frequency-regulation commitment. For all $t \in T$, if $\delta_t \geq 0$, then:

$$u_t = \max\left\{0, \delta_t n_{t-1} + d_{t-1} - c_{t-1} - l_{t-1}\right\}; \quad (1)$$

whereas if $\delta_t < 0$, then:

$$u_t = \min\left\{0, \delta_t n_{t-1} + d_{t-1} - c_{t-1} + \left(\bar{E} - l_{t-1}\right)/\eta\right\}; \quad (2)$$

where $\bar{E}$ is energy storage's maximum SOE (MWh) and η is its p.u. roundtrip efficiency. The intuition behind (1) is that if $\delta_t \geq 0$, energy storage must discharge $\delta_t n_{t-1}$ to fulfill its hour-$(t-1)$ frequency-regulation obligation. The maximum amount of energy that it could discharge, if it depletes it stored energy fully, is $(l_{t-1} - d_{t-1} + c_{t-1})$. u_t is the difference between these two quantities. The intuition behind (2) is analogous, but considers the amount that could be charged if energy-storage SOE goes to its maximum.

For all $t \in T$, if $\delta_{t+1} \geq 0$, then:

$$l_{t+1} = l_t + \eta c_t - (d_t + \delta_{t+1} n_t - u_{t+1}); \quad (3)$$

whereas if $\delta_{t+1} < 0$, then:

$$l_{t+1} = l_t + \eta \cdot (c_t - \delta_{t+1} n_t + u_{t+1}) - d_t. \quad (4)$$

To understand (3), suppose that $u_t = 0$, meaning that energy storage can fulfill its hour-$(t-1)$ frequency-regulation obligation. Because $\delta_{t+1} \geq 0$, energy storage must discharge $\delta_{t+1} n_t$ MWh. Combining this with its scheduled hour-t charging and discharging gives the right-hand side of (3). If energy storage is unable to fulfill its frequency-regulation obligation, the unfulfilled amount is deducted from the final term on the right-hand side of (3). State-transition function (4) has an analogous interpretation for cases wherein energy storage charges to fulfill its frequency-regulation obligation.

5) Constraints: The energy storage has power constraints:

$$0 \leq d_t + n_t \leq \bar{R}; \forall t \in T \quad (5)$$

$$0 \leq c_t + n_t \leq I_t \bar{R}/\eta; \forall t \in T; \quad (6)$$

where $\bar{R}$ is the power limit of the energy storage (MW); SOE constraints:

$$0 \leq l_{t+1} \leq \bar{E}; \forall t \in T; \quad (7)$$

and non-negativity constraints:

$$c_t, d_t, n_t \geq 0; \forall t \in T. \quad (8)$$

I_t appears in the right-hand side of (6) to ensure that energy storage does not charge during a loss of load. Constraints (7) can be rewritten as explicit restrictions on a_t, $\forall t \in T$, by using (3) and (4) to substitute for l_{t+1} in (7).

We define $\mathcal{A}_t(W_t, l_t)$, $\forall t \in T$, as the set of hour-t decisions that are feasible in (5)–(8) if the hour-t state is (W_t, l_t).

Some operational models of energy storage include explicit constraints to prevent simultaneous charging and discharging [36]. Such a restriction could be incorporated into our model easily, either by introducing binary variables or with logical constraints [34]. We do not include such constraints for two reasons. First, because of the η term that appears in (3) and (4), simultaneous charging and discharging is suboptimal under most cases [37]. Indeed, we do not observe simultaneous charging and discharging in our example nor in our case study. Second, some energy-storage technologies are capable of charging and discharging simultaneously [38]. Thus, a constraint preventing such operation would be unduly restrictive.

6) Objective-Contribution Functions: For all $t \in T$, the hour-t objective-contribution function is:

$$K_t(a_t; W_t, l_t) = \pi_t \cdot (d_t - c_t) + \rho_{t-1} n_{t-1} - \pi_{t-1} u_t/\delta_t - \bar{V} \cdot (1 - I_t)\left(\bar{R} - d_t\right); \quad (9)$$

which consists of four terms. The first gives net revenue that the energy storage earns from scheduled hour-t energy charging and discharging.

The next two terms give net revenue for providing frequency regulation. The term, $\rho_{t-1} n_{t-1}$, is revenue that energy storage earns from providing frequency-regulation capacity. The following term is the penalty for unfulfilled frequency-regulation deployments, which depends upon the energy price. This financial penalty is a common design of many wholesale electricity markets, and is used to incentivize resources to provide frequency regulation and other ancillary services in-line with their commitments [39]. The penalty cannot be levied until the dispatch-to-contract ratio is known, which is why these terms have the same one-hour lag that defines δ_t and u_t.

The final term that is in (9) gives the capacity-auction non-performance penalty, where $\bar{V}$ is the penalty cost (\$/MW-h). If there is an hour-t loss of load (*i.e.*, if $I_t = 0$), the energy storage is penalized if it discharges less than its rated power capacity. Otherwise, if $I_t = 1$, this term is zero.

Objective-contribution function (9) captures revenues, costs, and penalties that are related to energy-storage participation in the energy, frequency-regulation, and capacity markets. As such, our model captures the varying incentives of these markets on energy-storage operations and market participation.

7) Optimal Decision Policy: A feasible policy, ξ, is a mapping, $A_t^{\xi}(W_t, l_t)$, $\forall t \in T$, between an hour-t state, (W_t, l_t), and feasible hour-t decisions, $a_t \in \mathcal{A}_t(W_t, l_t)$. We define Ξ as the set of feasible policies and $\forall \xi \in \Xi, t \in T$ we define:

$$G_t^{\xi}(W_t, l_t) = \mathbb{E}\left[\sum_{\tau \in T, \tau \geq t} K_\tau(A_\tau^{\xi}(W_\tau, l_\tau); W_\tau, l_\tau) \middle| W_t\right];$$

as net energy-storage profit from hour t onward. If ξ^* satisfies:

$$G_t^{\xi^*}(W_t, l_t) = \sup_{\xi \in \Xi} G_t^{\xi}(W_t, l_t); \forall t \in T. \quad (10)$$

then it is an optimal decision policy. For all $t \in T$, we let:

$$c_t^{\xi^*}(W_t, l_t);$$

$$d_t^{\xi^*}(W_t, l_t);$$

and:

$$n_t^{\xi^*}(W_t, l_t);$$

denote optimal charging, discharging, and frequency-regulation policies, where we have:

$$A_t^{\xi^*}(W_t, l_t) = \left(c_t^{\xi^*}(W_t, l_t), d_t^{\xi^*}(W_t, l_t), n_t^{\xi^*}(W_t, l_t)\right).$$

B. Probability Distribution of l_t

For all $t \in T$ such that $t > 1$, l_t is random. This randomness is due to l_t depending upon charging, discharging, and frequency-regulation decisions, which depend upon the random state variables. In addition, l_t depends directly upon random state variables (*e.g.*, δ_t affects the values of u_t and l_t).

Using ξ^*, we can compute the probability distribution of l_t, $\forall t \in T$, which we denote as $\zeta_t(\cdot)$. To do so, we let $\bar{l}_1$ denote the starting hour-1 SOE and $\forall t \in T$, such that $t < |T|$ and $\delta_t \geq 0$, we define:

$$\mathcal{W}_{t+1}(y) = \Big\{ W_t, l_t \Big| l_t + \eta c_t^{\xi^*}(W_t, l_t) - \Big(d_t^{\xi^*}(W_t, l_t) + \delta_{t+1} n_t^{\xi^*}(W_t, l_t) - u_{t+1} \Big) = y \Big\}; \quad (11)$$

and $\forall t \in T$, such that $t < |T|$ and $\delta_t < 0$, we define:

$$\mathcal{W}_{t+1}(y) = \Big\{ W_t, l_t \Big| l_t + \eta \cdot \Big(c_t^{\xi^*}(W_t, l_t) - \delta_{t+1} n_t^{\xi^*}(W_t, l_t) + u_{t+1} \Big) - d_t^{\xi^*}(W_t, l_t) = y \Big\}. \quad (12)$$

For all $t \in T$, such that $t < |T|$, $\mathcal{W}_{t+1}(y)$ is defined as the set of hour-t states from which the optimal decision policy yields an hour-$(t+1)$ SOE of y MWh. With these definitions, we have:

$$\zeta_1(y) = \begin{cases} 1; & \text{if } y = \bar{l}_1 \\ 0; & \text{otherwise;} \end{cases} \quad (13)$$

and:

$$\zeta_{t+1}(y) = \int_{(\Gamma,\lambda) \in \mathcal{W}_{t+1}(y)} f_t(\Gamma) \zeta_t(\lambda) d\Gamma d\lambda; \quad \forall t \in T, t < |T|; \quad (14)$$

where $f_t(\cdot)$ is the joint probability distribution of W_t.

The intuition behind (13) is that the probability distribution of the hour-1 SOE is trivial—with probability 1 the SOE is $\bar{l}_1$. As for (14), consider an hour, $t \in T$, such that $t < |T|$. By the definition of $\mathcal{W}_{t+1}(y)$, for the hour-$(t+1)$ SOE to be a given value, y, the hour-t state variable must be an element of $\mathcal{W}_{t+1}(y)$. Equation (14) considers all elements, (Γ, λ), of the set, $\mathcal{W}_{t+1}(y)$, and for each one multiplies the probability that $W_t = \Gamma$ by the probability that $l_t = \lambda$. Integrating these products over the set, $\mathcal{W}_{t+1}(y)$, gives the probability that the hour-$(t+1)$ SOE is y. Equations (13) and (14) make no assumption about a parametric form for the probability distribution of the SOE. There may be cases that having a specified parametric form for $\zeta_t(y)$, $\forall t \in T$ is useful. Such an approximation could be achieved by fitting a parametric distribution to the distributions that are obtained from (13) and (14).

C. Energy-Storage ELCC

Resource-adequacy assessment may be done with different capacity-valuation and risk metrics [7]. Without loss of generality, we use ELCC and loss of load expectation (LOLE) as these two metrics. To compute energy-storage ELCC, first we calculate, $\forall t \in T$, the hour-t loss of load probability (LOLP) of the base electricity system (without energy storage) as:

$$p_t = \text{Prob}\{X_t < Z_t\}; \quad (15)$$

where X_t is hour-t generation capacity that is available (MW) and Z_t is hour-t demand (MW). The Prob$\{\cdot\}$ function that defines the LOLPs can account for any pertinent uncertainty (*e.g.*, generator failures). By definition, $\forall t \in T$, p_t and $(1-p_t)$ are the probabilities with which I_t equals 0 and 1, respectively. The LOLE of the base system is defined as:

$$\sum_{t \in T} p_t.$$

Energy-storage ELCC is defined as the value of $\bar{Z}$ such that:

$$\sum_{t \in T} p_t = \sum_{t \in T} \int_{\lambda=0}^{\bar{E}} \int_{\Gamma} f_t(\Gamma) \zeta_t(\lambda) \times \text{Prob}\Big\{ X_t + d_t^{\xi^*}(\Gamma, \lambda) < Z_t + \bar{Z} \Big\} d\Gamma d\lambda. \quad (16)$$

The intuition behind (16) is that energy storage increases electricity-system reliability, insomuch as it may discharge during a loss of load. This discharging is reflected on the left-hand side of the inequality that is in the Prob$\{\cdot\}$ function in (16). The amount that is discharged during each hour depends, through ξ^*, on W_t and l_t. Thus, the probability distributions, $f_t(\Gamma)$ and $\zeta_t(\lambda)$, of these random variables appear in the integrand. The ELCC, $\bar{Z}$, is the amount by which the hourly loads can be increased to achieve the same LOLE of the system with the energy storage as that of the base system.

III. Approximate Model

The approach that is outlined in Section II is exact but computationally intractable due to two complicating factors. First, the stochastic dynamic optimization has large (potentially uncountably infinite) decision- and state-variable spaces. Second, (11), (12), (14), and (16) involve sets and integrals that likely cannot be computed directly. Thus, we propose the following three-step process to approximate the exact model, which employs discretized optimization and random sampling. The approximation is exact, in the sense that it should replicate the outcomes of the exact model if the discretization and random sampling are exact (*i.e.*, replicate the true underlying decision and state spaces and random variables). We demonstrate this exactness empirically with our example in Section V-A. Fig. 1 is a high-level flow chart that summarizes the connections between the three steps. As we describe each step of the modeling process, we explain the steps and linkages that are shown by Fig. 1.

A. Discretized Stochastic Dynamic Optimization

Step 1 of our method (*cf.* Fig. 1) employs a discretized version of the model that is proposed in Section II-A [40]. All of T, t, π_t, ρ_t, I_t, and δ_t retain the same definitions as before. For all $t \in T$, we define $\tilde{c}_t$, $\tilde{d}_t$, $\tilde{n}_t$, $\tilde{a}_t$, $\tilde{u}_t$, and $\tilde{l}_t$ as discretized variants of c_t, d_t, n_t, a_t, u_t, and l_t, respectively. The discretization that is used is a modeling choice, which

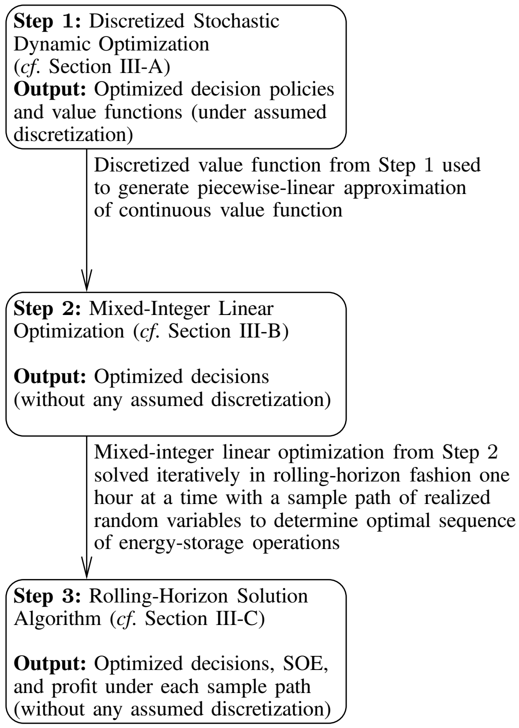

Fig. 1. High-level flow chart of the three-step approximation method that is outlined in Section III.

introduces a tradeoff between computational complexity and fidelity of the model results. Section IV details the discretization that we use in our example and case study, which performs well *vis-à-vis* the aforementioned tradeoff. For notational ease, $\forall t \in T$, we let M_t denote the number of values that $\tilde{l}_t$ can take in the discretization and let $\tilde{l}_t^1 \leq \tilde{l}_t^2 \leq \cdots \leq \tilde{l}_t^{M_t}$ denote the values to which $\tilde{l}_t$ is restricted. For all $t \in T$, we define:

$$\tilde{W}_t = (\pi_t, \rho_t, I_t, \delta_t, \tilde{u}_t)\,;$$

let Ω_t denote the set of scenarios for the exogenous hour-t state variables, and let ω be the scenario index. As needed, an ω superscript indicates the scenario-ω value of a state variable.

The exogenous state variables are simulated (*cf.* Sections II-C and IV) and the endogenous state variables follow the same state transitions that are given in (1)–(4), with tildes on appropriate terms. The discretized model includes the same constraints, (5)–(8), with tildes on appropriate terms.

For all $t \in T$, the hour-t objective-contribution function of the discretized model is:

$$\begin{aligned}\tilde{K}_t(\tilde{a}_t; \tilde{W}_t, \tilde{l}_t) = \pi_t \cdot \left(\tilde{d}_t - \tilde{c}_t\right) + \rho_{t-1}\tilde{n}_{t-1} - \pi_{t-1}\tilde{u}_t/\delta_t \\ - \bar{V} \cdot (1 - I_t)\left(\bar{R} - \tilde{d}_t\right) - \pi_t \cdot (\delta_{t+1}\tilde{n}_t - S_i). \quad (17)\end{aligned}$$

The first four terms of (9) and (17) are identical, save for tildes in the latter. The fifth term in (17) is a correction factor, which accounts for $\tilde{l}_{t+1}$ being restricted to one of $\tilde{l}_t^1, \tilde{l}_t^2, \cdots, \tilde{l}_t^{M_t}$. Specifically, the amount of energy that must be supplied to fulfill the frequency-regulation obligation, $\delta_{t+1}\tilde{n}_t$, is rounded to an element of the ordered set, $\mathcal{S}$. We define S_i in (17) as:

$$\arg\min_{S \in \mathcal{S}} |\delta_{t+1}\tilde{n}_t - S|\,.$$

Thus, the fifth term in (17) assumes that the rounding error in the frequency-regulation obligation is settled through the energy market.

We define $\tilde{\xi}$, $\tilde{\Xi}$, and $\tilde{G}_t^{\tilde{\xi}}(\tilde{W}_t, \tilde{l}_t)$, $\forall t \in T$ analogously to ξ, Ξ, and $G_t^{\xi}(W_t, l_t)$, respectively, with tildes on appropriate terms. Thus, $\tilde{\xi}^*$ is an optimal decision policy if it satisfies:

$$\tilde{G}_t^{\tilde{\xi}^*}(\tilde{W}_t, \tilde{l}_t) = \sup_{\tilde{\xi} \in \tilde{\Xi}} \tilde{G}^{\tilde{\xi}_t}(\tilde{W}_t, \tilde{l}_t); \forall t \in T.$$

Because of the assumed finite decision- and state-variable spaces, $\tilde{\xi}^*$ can be obtained using backward recursion.

As noted above, the discretized stochastic dynamic optimization gives the same decision policies as the model that is introduced in Section II-A if the discretization is exact in the sense that it represents the true decision and state spaces and random variables. This exactness is because the fifth term in (17) becomes zero, which means that the objective-contribution functions and constraints of the discretized and exact dynamic optimizations are the same.

B. Mixed-Integer Linear Optimization

As is stated in the box that is labled 'Step 1' in Fig. 1, $\tilde{\xi}^*$ is optimal if the energy storage is restricted to the assumed discretization. Our numerical results suggest that a discretization that yields a computationally tractable dynamic optimization gives poor ELCC estimates. Thus, our second step uses:

$$\tilde{G}_{t+1}^{\tilde{\xi}^*}(\tilde{W}_{t+1}, \tilde{l}_{t+1}), \forall t \in T;$$

in a two-stage stochastic mixed-integer linear optimization that relaxes the discretization. This linkage between Steps 1 and 2 is illustrated by the arrow connecting the two corresponding boxes that are in Fig. 1. This model determines energy-storage operations in a rolling-horizon fashion (*cf.* Section III-C). For all $t \in T$, the hour-t model optimizes a_t and uses a piecewise-linear approximation of:

$$\tilde{G}_{t+1}^{\tilde{\xi}^*}(\tilde{W}_{t+1}, \tilde{l}_{t+1});$$

to tradeoff between a_t and subsequent decisions.

For all $t \in T$, we have that:

$$\tilde{G}_{t+1}^{\tilde{\xi}^*}(\tilde{W}_{t+1}, \tilde{l}_{t+1});$$

depends on hour-t and -$(t+1)$ decision variables. To use:

$$\tilde{G}_{t+1}^{\tilde{\xi}^*}(\tilde{W}_{t+1}, \tilde{l}_{t+1}), \forall t \in T;$$

in the fashion that we envision, we need to have terms that depend on hour-$(t{+}1)$ variables only. Thus, $\forall t \in T$, we define:

$$\begin{aligned}\tilde{G}_{t+1}^*(\tilde{W}_{t+1}, \tilde{l}_{t+1}) = \\ \pi_{t+1} \cdot \left(d_{t+1}^{\tilde{\xi}^*}\left(\tilde{W}_{t+1}, \tilde{l}_{t+1}\right) - c_{t+1}^{\tilde{\xi}^*}\left(\tilde{W}_{t+1}, \tilde{l}_{t+1}\right)\right) \\ + \rho_{t+1} n_{t+1}^{\tilde{\xi}^*}\left(\tilde{W}_{t+1}, \tilde{l}_{t+1}\right) - \pi_{t+1}\tilde{u}_{t+2}/\delta_{t+2} \\ - \bar{V} \cdot (1 - I_t)\left(\bar{R} - d_{t+1}^{\tilde{\xi}^*}\left(\tilde{W}_{t+1}, \tilde{l}_{t+1}\right)\right) \\ + \tilde{G}_{t+2}^*\left(\tilde{W}_{t+2}, \tilde{l}_{t+2}\right).\end{aligned}$$

For all $t \in T$, based on (9) and the one-hour offset in defining δ_t and u_t, we have that:

$$\tilde{G}^{\tilde{\xi}^*}_{t+1}(\tilde{W}_{t+1}, \tilde{l}_{t+1});$$

includes the term, $\rho_t n_t - \pi_t \tilde{u}_{t+1}/\delta_{t+1}$. The function:

$$\tilde{G}^*_{t+1}(\tilde{W}_{t+1}, \tilde{l}_{t+1})$$

replaces this term with $\rho_{t+1} n_{t+1} - \pi_{t+1}\tilde{u}_{t+2}/\delta_{t+2}$. This time-index change does not affect the overall objective function, as all of $\rho_1 n_1, \ldots, \rho_{|T|} n_{|T|}$ and $\pi_1 \tilde{u}_2/\delta_2, \ldots, \pi_T \tilde{u}_{|T|+1}/\delta_{|T|+1}$ are considered in the rolling-horizon optimization. With this definition, $\forall t \in T$, $m = 1, \ldots, M_t - 1$, we can define the slope of the mth piece of the piecewise-linear interpolation of $\tilde{G}^*_{t+1}(\tilde{W}_{t+1}, \tilde{l}_{t+1})$ as:

$$\hat{\sigma}^m_{t+1}(\tilde{W}_{t+1}) = \frac{\tilde{G}^*_{t+1}(\tilde{W}_{t+1}, \tilde{l}^{m+1}_{t+1}) - \tilde{G}^*_{t+1}(\tilde{W}_{t+1}, \tilde{l}^m_{t+1})}{\tilde{l}^{m+1}_t - \tilde{l}^m_t}. \quad (18)$$

Our mixed-integer linear model optimizes hour-t energy-storage operations, c_t, d_t, n_t. Depending upon the scenario, $\omega \in \Omega_{t+1}$, that is realized, the random variable, δ^ω_{t+1}, determines the amount of energy that must be supplied to fulfill the frequency-regulation obligation. These values determine the resultant unfulfilled frequency-regulation energy, u^ω_{t+1}, and SOE, l^ω_{t+1}. In addition to c_t, d_t, n_t, and u^ω_{t+1} and l^ω_{t+1}, $\forall \omega \in \Omega_{t+1}$, the model has two additional auxiliary-variable sets, which are used for the piecewise-linear approximation of $\tilde{G}^*_{t+1}(\tilde{W}_{t+1}, \tilde{l}_{t+1})$. Specifically, $\forall \omega \in \Omega_{t+1}$, we break l^ω_{t+1} into segments that correspond to the values to which $\tilde{l}_{t+1}$ is restricted in the discrete dynamic optimization. For all $m = 1, \ldots, M_{t+1}$ and $\omega \in \Omega_{t+1}$, $y^{m,\omega}_{t+1}$ is a binary variable that equals 1 if $l^\omega_{t+1} \geq \tilde{l}^m_{t+1}$ and equals 0 otherwise. For all $m = 1, \ldots, M_{t+1} - 1$ and $\omega \in \Omega_{t+1}$, $q^{m,\omega}_{t+1}$ is defined as the amount of l^ω_{t+1} that is greater than or equal to $\tilde{l}^m_{t+1}$ and less than or equal to $\tilde{l}^{m+1}_{t+1}$.

The mixed-integer linear model is formulated as:

$$\max\ \pi_t \cdot (d_t - c_t) + \rho_t n_t - \bar{V} \cdot (1 - I_t)\left(\bar{R} - d_t\right) + \sum_{\omega \in \Omega_{t+1}} \text{Prob}\left\{W^\omega_{t+1} | W_t\right\} \times \sum_{m=1}^{M_t - 1} \left(\hat{\sigma}^m_{t+1}(W^\omega_{t+1}) q^{m,\omega}_{t+1} - \pi_t \frac{u^\omega_{t+1}}{\delta^\omega_{t+1}}\right) \quad (19)$$

$$\text{s.t. } 0 \leq d_t + n_t \leq \bar{R} \quad (20)$$

$$0 \leq c_t + n_t \leq I_t \bar{R}/\eta \quad (21)$$

$$0 \leq l^\omega_{t+1} \leq \bar{E}; \forall \omega \in \Omega_{t+1} \quad (22)$$

$$u^\omega_{t+1} \geq 0; \forall \omega \in \Omega_{t+1} \ni \delta^\omega_{t+1} \geq 0 \quad (23)$$

$$u^\omega_{t+1} \geq \delta^\omega_{t+1} n_t + d_t - c_t - l_t; \quad \forall \omega \in \Omega_{t+1} \ni \delta^\omega_{t+1} \geq 0 \quad (24)$$

$$u^\omega_{t+1} \leq 0; \forall \omega \in \Omega_{t+1} \ni \delta^\omega_{t+1} < 0 \quad (25)$$

$$u^\omega_{t+1} \leq \delta^\omega_{t+1} n_t + d_t - c_t + \left(\bar{E} - l_t\right)/\eta; \quad \forall \omega \in \Omega_{t+1} \ni \delta^\omega_{t+1} < 0 \quad (26)$$

$$u^\omega_{t+1} \leq I_t \bar{R}; \forall \omega \in \Omega_{t+1} \ni \delta^\omega_{t+1} \geq 0 \quad (27)$$

$$u^\omega_{t+1} \leq I_t \bar{R}; \forall \omega \in \Omega_{t+1} \ni \delta^\omega_{t+1} < 0 \quad (28)$$

$$l^\omega_{t+1} = l_t + \eta c_t - \left(d_t + \delta^\omega_{t+1} n_t - u^\omega_{t+1}\right); \quad \forall \omega \in \Omega_{t+1} \ni \delta^\omega_{t+1} \geq 0 \quad (29)$$

$$l^\omega_{t+1} = l_t + \eta \cdot \left(c_t - \delta^\omega_{t+1} n_t + u^\omega_{t+1}\right) - d_t; \quad \forall \omega \in \Omega_{t+1} \ni \delta^\omega_{t+1} < 0 \quad (30)$$

$$\sum_{m=1}^{M_{t+1}-1} q^{m,\omega}_{t+1} = l^\omega_{t+1}; \forall \omega \in \Omega_{t+1} \quad (31)$$

$$0 \leq q^{m,\omega}_{t+1} \leq y^{m,\omega}_{t+1} \cdot \left(\tilde{l}^{m+1}_{t+1} - \tilde{l}^m_{t+1}\right); \quad \forall \omega \in \Omega_{t+1}; m = 1, \ldots, M_{t+1} - 1 \quad (32)$$

$$q^{m,\omega}_{t+1} \geq y^{m+1,\omega}_{t+1} \cdot \left(\tilde{l}^{m+1}_{t+1} - \tilde{l}^m_{t+1}\right); \quad \forall \omega \in \Omega_{t+1}; m = 1, \ldots, M_{t+1} - 1 \quad (33)$$

$$y^{m,\omega}_{t+1} \in \{0, 1\}; \forall \omega \in \Omega_{t+1}; m = 1, \ldots, M_{t+1} \quad (34)$$

$$c_t, d_t, n_t \geq 0; \quad (35)$$

Objective function (19) is a linear Bellman-like equation that consists of immediately earned net profit from the hour-t decisions (the first three terms) and expected profit that is earned from hour $(t+1)$ onward. The expected-profit term uses the slopes that are computed in (18) to give a piecewise-linear approximation of $\tilde{G}^*_{t+1}(W^\omega_{t+1}, l^\omega_{t+1})$, $\forall \omega \in \Omega_{t+1}$. The use of $\tilde{G}^*_{t+1}(\tilde{W}_{t+1}, \tilde{l}_{t+1})$ in defining these slopes yields immediate-profit terms that depend solely upon hour-t decisions.

Constraints (20)–(22) and (35) are analogous to (5)–(8) in the exact model and (23)–(26) are analogous to (1)–(2). The $\min\{\cdot\}$ and $\max\{\cdot\}$ operators that appear in (1)–(2) are linearized in (23)–(26) using pairs of inequalities. For all $\omega \in \Omega_{t+1}$, energy storage is penalized for having non-zero values of u^ω_{t+1}. Thus, an optimal solution that satisfies (23)–(26) satisfies (1)–(2). For all $\omega \in \Omega_{t+1}$, (29)–(30) use the values of u^ω_{t+1} that are determined by (23)–(26) to determine the hour-$(t+1)$ SOE. Constraints (27) and (28) ensure that unserved frequency regulation is zero if $I_t = 0$, because, by assumption, energy storage does not provide frequency regulation during a loss of load.

Constraints (31)–(34) pertain to the piecewise-linear approximation of $\tilde{G}^*_{t+1}(W^\omega_{t+1}, l^\omega_{t+1})$, $\forall \omega \in \Omega_{t+1}$. For all $\omega \in \Omega_{t+1}$, (31) decomposes l^ω_{t+1} into the sum over $m = 1, \ldots, M_{t+1} - 1$ of $q^{m,\omega}_{t+1}$. For all $\omega \in \Omega_{t+1}$ and $m = 1, \ldots, M_{t+1} - 1$, (32) restricts $q^{m,\omega}_{t+1}$ to equal zero if $y^{m,\omega}_{t+1} = 0$. Otherwise, if $y^{m,\omega}_{t+1} = 1$, then $q^{m,\omega}_{t+1}$ is restricted to be no greater than $(\tilde{l}^{m+1}_{t+1} - \tilde{l}^m_{t+1})$. For all $\omega \in \Omega_{t+1}$ and $m = 1, \ldots, M_{t+1} - 1$, (33) forces $q^{m,\omega}_{t+1}$ to equal $(\tilde{l}^{m+1}_{t+1} - \tilde{l}^m_{t+1})$ if $y^{m+1,\omega}_{t+1} = 1$. Finally, (34) imposes integrality restrictions on all $y^{m,\omega}_{t+1}$.

C. Rolling-Horizon Solution Algorithm

The final step of our approximation method solves (19)–(35) in a rolling-horizon fashion one hour at a time to determine the contribution of energy storage towards mitigating a loss of load. Specifically, two key outputs are computed. The first, $\breve{\zeta}_t(\cdot)$, $\forall t \in T$, is the approximated probability distribution of the hour-t energy-storage SOE. The second, $\breve{d}^{\omega,l_t}_t$, $\forall t \in T, \omega \in \Omega_t, l_t = \tilde{l}^1_t, \ldots, \tilde{l}^{M_t}_t$ is the amount that energy storage discharges during hour t if there is an hour-t loss of load and the hour-t exogenous state and starting energy-storage SOE are

ω and l_t, respectively. Once these quantities are determined, an ELCC calculation that is akin to (16) is conducted. The linkage between Steps 2 and 3 are illustrated by the corresponding arrow in Fig. 1, which summarizes also the outputs of the rolling-horizon algorithm.

Our method solves (19)–(35) in a rolling-horizon fashion because, by its structure, each instance of (19)–(35) provides optimized decisions for a single hour only. Thus, solving (19)–(35) in a rolling-horizon fashion yields a sequence of optimized decisions. Alternatively, (19)–(35) could be structured to represent explicitly the full sequence of decisions. However, such a formulation would result in a large and computationally intractable multi-stage stochastic mixed-integer linear optimization.

Algorithm 1 provides pseudocode for the rolling-horizon technique. Line 1 initializes the algorithm by setting $\breve{\zeta}_t(\cdot)$ equal to zero $\forall t \in T$ and Line 2 sets the boundary condition by setting $\breve{\zeta}_1(\bar{l}_1)$ equal to 1, which is akin to (13). The algorithm iterates through each hour of the model horizon (*cf.* Line 3) and $\forall t \in T$, each discrete hour-t exogenous state (*cf.* Line 4).

For all $t \in T \ni t > 1$, Lines 5–20 conduct an iterative updating of $\breve{\zeta}_t(\cdot)$ that is akin to (14). Lines 5–20 are unnecessary for $t = 1$, because $l_1 = \bar{l}_1$ with probability 1 (*cf.* Line 2). Lines 5–20 examine all possible hour-$(t-1)$ exogenous state variable-values (*cf.* Line 6) and all possible hour-$(t-1)$ SOE levels (*cf.* Line 7). For each state-variable/SOE pair, unserved frequency-regulation energy is computed in Line 9 or 12 and the resultant starting hour-t SOE is computed in Line 10 or 13 (depending on whether energy storage discharges or charges to serve frequency regulation). These calculations depend upon an optimal set of hour-$(t-1)$ decisions, $\dot{c}_{t-1}^{\omega,l_{t-1}}$, $\dot{d}_{t-1}^{\omega,l_{t-1}}$, and $\dot{n}_{t-1}^{\omega,l_{t-1}}$, which are determined by Line 22. Line 15 computes the resultant hour-t contribution to the overall energy-storage objective function. This computation is not necessary for resource-adequacy assessment, but is included to assess financial performance. Line 16 rounds $\breve{l}_t^{\omega',l_{t-1}}$ to the nearest value among the hour-t discretization, $\tilde{l}_t^1, \ldots, \tilde{l}_t^{M_t}$. Line 17 is the recursive updating of $\breve{\zeta}_t(\cdot)$.

Once $\breve{\zeta}_t(\cdot)$ is updated, Lines 21–29 conduct two calculations for each possible discrete hour-t starting SOE level. First, Line 22 solves (19)–(35) to determine an optimal set of hour-t decisions, given the actual exogenous hour-t state. Next, Lines 23–27 determine energy storage's discharging action if there is an hour-t loss of load. Line 24 considers the case in which the capacity auction requires that energy storage supply as much energy as it is technically capable of supplying. Line 27 assumes no such requirement and determines energy-storage action by solving (19)–(35) with I_t fixed equal to 0.

Following from the discussion that is in Section III-A, solving (19)–(35) using Algorithm 1 yields:

$$\zeta_t(l) = \breve{\zeta}_t(l), \forall t \in T, l;$$

which means that the exact and approximate model are equivalent, if the discretization that is used is exact. This equivalence stems from (19) being the same linear Bellman-like equation that would be used to solve (10) and the feasible space that is defined by (20)–(35) being the same as $\mathcal{A}_t(W_t, l_t)$, $\forall t \in T$.

Algorithm 1 Rolling-Horizon Algorithm for (19)–(35)

1: $\breve{\zeta}_t(l_t) \leftarrow 0, \forall t \in T$
2: $\breve{\zeta}_1(\bar{l}_1) \leftarrow 1$
3: **for** $t \in T$ **do**
4: **for** $\omega \in \Omega_t$ **do**
5: **if** $t > 1$ **then**
6: **for** $\omega' \in \Omega_{t-1}$ **do**
7: **for** $l_{t-1} \leftarrow \tilde{l}_{t-1}^1$ to $\tilde{l}_{t-1}^{M_{t-1}}$ **do**
8: **if** $\delta_t^\omega \geq 0$ **then**
9: $\breve{u}_t^{\omega',l_{t-1}} \leftarrow \max\{0, \delta_t^\omega \dot{n}_{t-1}^{\omega',l_{t-1}} + \dot{d}_{t-1}^{\omega',l_{t-1}} - \dot{c}_{t-1}^{\omega',l_{t-1}} - l_{t-1}\}$
10: $\breve{l}_t^{\omega',l_{t-1}} \leftarrow l_{t-1} + \eta \dot{c}_{t-1}^{\omega',l_{t-1}} - (\dot{d}_{t-1}^{\omega',l_{t-1}} + \delta_t^\omega \dot{n}_{t-1}^{\omega',l_{t-1}} - \breve{u}_t^{\omega',l_{t-1}})$
11: **else**
12: $\breve{u}_t^{\omega',l_{t-1}} \leftarrow \min\{0, \delta_t^\omega \dot{n}_{t-1}^{\omega',l_{t-1}} + \dot{d}_{t-1}^{\omega',l_{t-1}} - \dot{c}_{t-1}^{\omega',l_{t-1}} + (\bar{E} - l_{t-1})/\eta\}$
13: $\breve{l}_t^{\omega',l_{t-1}} \leftarrow l_{t-1} + \eta \cdot (\dot{c}_{t-1}^{\omega',l_{t-1}} - \delta_t^\omega \dot{n}_{t-1}^{\omega',l_{t-1}} + \breve{u}_t^{\omega',l_{t-1}}) - \dot{d}_{t-1}^{\omega',l_{t-1}}$
14: **end if**
15: $\breve{K}_{t-1}^{\omega',l_{t-1}} \leftarrow \pi_{t-1}^{\omega'} \cdot (\dot{d}_{t-1}^{\omega',l_{t-1}} - \dot{c}_{t-1}^{\omega',l_{t-1}} - \breve{u}_t^{\omega',l_{t-1}}/\delta_t^\omega) + \rho_{t-1}^{\omega'} \dot{n}_{t-1}^{\omega',l_{t-1}} - \bar{V} \cdot (1 - I_{t-1})(\bar{R} - \dot{d}_{t-1}^{\omega',l_{t-1}})$
16: $\breve{l}_t^{\omega',l_{t-1}} \leftarrow \arg\min_{l_t \in \{\tilde{l}_t^1, \ldots, \tilde{l}_t^{M_t}\}} |l_t - \breve{l}_t^{\omega',l_{t-1}}|$
17: $\breve{\zeta}_t(\breve{l}_t^{\omega',l_{t-1}}) \leftarrow \breve{\zeta}_t(\breve{l}_t^{\omega',l_{t-1}}) + \breve{\zeta}_{t-1}(l_{t-1}) \times \text{Prob}\left\{W_t^\omega | W_{t-1}^{\omega'}\right\} \text{Prob}\left\{W_{t-1}^{\omega'}\right\}$
18: **end for**
19: **end for**
20: **end if**
21: **for** $l_t \leftarrow \tilde{l}_t^1$ to $\tilde{l}_t^{M_t}$ **do**
22: $(\dot{c}_t^{\omega,l_t}, \dot{d}_t^{\omega,l_t}, \dot{n}_t^{\omega,l_t}) \leftarrow \arg\max$ (19) s.t. (20)–(35)
23: **if** $\bar{V} > 0$ **then**
24: $\ddot{c}_t^{\omega,l_t} \leftarrow 0$, $\ddot{d}_t^{\omega,l_t} \leftarrow \min\{l_t, \bar{R}\}$, $\ddot{n}_t^{\omega,l_t} \leftarrow 0$
25: **else**
26: $I_t^\omega \leftarrow 0$
27: $(\ddot{c}_t^{\omega,l_t}, \ddot{d}_t^{\omega,l_t}, \ddot{n}_t^{\omega,l_t}) \leftarrow \arg\max$ (19) s.t. (20)–(35)
28: **end if**
29: **end for**
30: **end for**
31: **end for**

Because (19)–(35) is solved in a rolling-horizon fashion, it replicates the application of dynamic programming algorithm to solve (10) [34].

D. Estimated Energy-Storage ELCC

To estimate energy-storge ELCC, we begin by using (15) to compute the LOLPs of the base system (without energy storage). The estimated energy-storage ELCC is defined as the value of $\bar{Z}$ such that:

$$\sum_{t \in T} p_t = \sum_{t \in T} \sum_{\omega \in \Omega_t} \sum_{\omega' \in \Omega_{t-1}} \sum_{l_t \in \{\tilde{l}_t^1, \ldots, \tilde{l}_t^{M_t}\}} \breve{\zeta}_t(l_t)$$

$$\times \text{Prob}\left\{W_t^{\omega}\,\middle|\,W_{t-1}^{\omega'}\right\}\text{Prob}\left\{W_{t-1}^{\omega'}\right\}$$
$$\times \text{Prob}\left\{X_t+\ddot{d}_t^{\omega,l_t}<Z_t+\bar{Z}\,\middle|\,W_t^{\omega}\right\}. \quad (36)$$

The values, $\breve{\zeta}_t(\cdot)$, $\forall t \in T$ and $\ddot{d}_t^{\omega,l_t}$, $\forall t \in T, \omega \in \Omega_t, l_t = \tilde{l}_t^1, \ldots, \tilde{l}_t^{M_t}$, which appear in (36) are obtained from Algorithm 1, as is listed in the 'Outputs' of 'Step 3' in Fig. 1. The ELCC calculations that are given by (16) and (36) are equivalent if the discretization that is used is exact. This result follows immediately from the discussions in Sections III-A and III-C regarding the equivalence of the stochastic dynamic optimization that is detailed in Section II-A and the three-step approximation method.

IV. Data Generation and Simulation

We apply our model to a case study that is based on historical real-world data that are obtained from the operator of a summer-peaking electricity system [13]. Due to data propriety, we are able neither to provide the raw data nor to reveal the system to which the data correspond. We summarize the raw data and the steps that are taken to construct our case study.

We use nine data sets. Two of the data sets—nameplate generator capacities and hourly net loads (*i.e.*, demand less renewable-generator and behind-the-meter power output)—are combined with generator effective forced outage rates (EFORs) to compute hourly LOLPs. EFORs represent generators' steady-state unavailability probabilities, accounting for restoration time after a failure occurs. The other seven data sets are summarized in Table I. Except for frequency-regulation deployments, all of the data sets that are listed in Table I have hourly resolutions. Frequency-regulation deployments are reported at four-second intervals, and the values are integrated numerically to yield hourly values. The second column of Table I specifies the fitted parametric distribution of each data set, which is determined using Anderson-Darling tests [41].

TABLE I
Raw Data Used to Construct Case Study and Fitted Parametric Distribution of Each Data Set

Data Set	Fitted Distribution
Energy Price	Gamma
Upward Frequency-Regulation Price	Log-Normal
Downward Frequency-Regulation Price	Log-Normal
Upward Frequency-Regulation Procurement	Log-Normal
Downward Frequency-Regulation Procurement	Log-Normal
Upward Frequency-Regulation Deployment	Weibull
Downward Frequency-Regulation Deployment	Weibull

The exogenous random variables, π_t, ρ_t, and δ_t, are simulated from the fitted distributions by bootstrapping [42] and employing one-step-ahead forecasting [43], [44]. We illustrate the simulation process for π_t, $\forall t \in T$. For all $t \in T$, we define $\pi_{t+1} = \pi_t + \Delta\pi_t$, where $\Delta\pi_t$ follows a fitted gamma distribution (as specified in Table I). Randomly sampling a value of $\Delta\pi_t$ using the fitted gamma distribution gives a randomly generated value of π_{t+1}. In addition, π_t, $\forall t \in T$ is Markovian, which captures serial correlations in the underlying data set. For all $t \in T$, ρ_t is simulated identically.

For all $t \in T$, δ_t is defined as the ratio between the frequency-regulation deployment and procurement. As such, $\forall t \in T$, we generate one random sample each of upward and downward frequency-regulation deployments and procurements using the same simulation procedure that is used to generate π_t and ρ_t, $\forall t \in T$. The ratios between the deployments and procurements of upward and downward frequency regulation are computed and the larger of the two ratios is used for the simulated value of δ_t and the associated frequency-regulation price is used as the corresponding value of ρ_t (*i.e.*, we take a conservative approach, wherein a worst-case value of δ_t that requires the most energy deployment is realized).

For all $t \in T$, I_t is simulated by conducting Bernoulli trials of generator failures. Specifically, during each hour, each generator is assumed to have a failure, in which case it has zero capacity available, with probability equal to its EFOR. Otherwise, if a generator does not have a failure, its nameplate capacity is available. For a given sample of Bernoulli trials, LOLPs can be computed using (15).

For all $t \in T$, we generate 49 equiprobable samples of the random variables. k-means clustering is applied to reduce the 49 samples to seven clusters, using cluster centroids as the associated random-variable values. For all $t \in T$, the transition probability between hour-$(t-1)$ cluster, i, and hour-t cluster, j, is determined by the number of transitions that occur between the elements of clusters i and j [45]. Specifically, $\forall t \in T$, let $\phi_{i,j}^t$ denote the number of transitions from elements of cluster i to elements of cluster j. The probability of transitioning from cluster i during hour $(t-1)$ to cluster j during hour t is:

$$\phi_{i,j}^t \Big/ \sum_{k\in\kappa_t}\phi_{i,k}^t;$$

where κ_t is the set of hour-t clusters. Student's t-test and Levene's test are used to verify the goodness of fit of the simulated data to the underlying raw data sets.

Finally, $\forall t \in T$, one sample from the reduced clusters is selected randomly to represent the 'actual' realized sample path of the random variables.

We assume that $\bar{R} = 100$ MW, $\eta = 0.75$, and consider different values of $\bar{E}$ and $\bar{V}$. The discretized stochastic dynamic optimization allows each of $\eta\tilde{c}_t$, $\tilde{d}_t$, and $\tilde{n}_t$, $\forall t \in T$ to take one of 101 equally spaced values between their lower and upper bounds. For all $t \in T$, $\tilde{l}_t$ is discretized between its minimum and maximum value using 1-MWh increments. For all $t \in T$, the piecewise-linear interpolation of $\tilde{G}_{t+1}^*(\tilde{W}_{t+1}, \tilde{l}_{t+1})$ requires discretization of $\tilde{l}_t$, which is discretized between its minimum and maximum values using 5-MWh increments.

For all of our computations, Algorithm 1 is implemented using MATLAB 2022. The optimization problems that are solved in Lines 22 and 27 are programmed using GAMS 40.0 and solved using CPLEX 22.1.1.0. Computations are done using a computer with an Intel $i7-11700$ CPU and 16 GB of memory.

V. Numerical Example

We begin by examining a simple example that considers the single day with the highest LOLPs of the case-study year.

A. Case 1: Model Benchmarking

We begin with a case that assumes the energy storage does not provide frequency regulation (*i.e.*, all frequency-regulation-related variables are fixed equal to zero) and that there is no price uncertainty. This case benchmarks our approximation technique to an exact model [13] that captures neither frequency regulation nor price uncertainty. In doing so, we are able to demonstrate the theoretical equivalence between the exact model and three-step approximation, by virtue of our using a sufficiently granular discretization. Table II summarizes the sample means and standard errors of ELCCs that are obtained from applying the exact model to 100 replications of the data-generation process that is summarized in Section IV. Table III summarizes the same outputs from applying our approximation technique to the same 100 replications. Using the values that are reported in the tables, we conduct hypothesis tests to determine whether the mean ELCCs are statistically significantly different. In all cases, we are unable to reject the null hypothesis at the 1% confidence level, which provides strong evidence that the two models provide ELCC estimates that are statistically similar.

TABLE II
MEAN AND STANDARD ERROR (IN PARENTHESES) ELCC OF ENERGY STORAGE (% OF NAMEPLATE NET DISCHARGING CAPACITY) IN EXAMPLE FROM SECTION V-A USING EXACT MODEL [13]

	$\bar{V}$		
$\bar{E}$	0	1000	9000
100	30 (0.03)	85 (0.01)	85 (0.00)
200	59 (0.00)	97 (0.01)	98 (0.00)
400	78 (0.60)	99 (0.01)	99 (0.02)
800	100 (0.07)	100 (0.00)	100 (0.00)

TABLE III
MEAN AND STANDARD ERROR (IN PARENTHESES) ELCC OF ENERGY STORAGE (% OF NAMEPLATE NET DISCHARGING CAPACITY) IN EXAMPLE FROM SECTION V-A USING APPROXIMATION

	$\bar{V}$		
$\bar{E}$	0	1000	9000
100	30 (0.03)	85 (0.01)	85 (0.00)
200	59 (0.00)	97 (0.01)	98 (0.00)
400	79 (0.65)	99 (0.01)	99 (0.03)
800	100 (0.00)	100 (0.00)	100 (0.00)

The tables show that increasing either of $\bar{V}$ or $\bar{E}$ increases energy-storage ELCC [13]. The former is due to energy storage being operated to have a higher SOE during high-LOLP hours and the latter due to the energy storage having greater energy-carrying capacity.

B. Case 2: Price Uncertainty

Our second case is the same as Case 1, except that we model price uncertainty. We cannot benchmark our approximation to the exact model, because the latter does not represent price uncertainty [13]. Thus, we examine this case by comparing energy-storage ELCC estimates that are obtained from our proposed approximation with and without price uncertainty. Table IV summarizes the means and standard errors of the Case-2 ELCC estimates that are obtained from applying our approximation method to the same 100 replications that are examined in Section V-A. Using the results that are reported in Tables III and IV, we conduct hypothesis tests to determine if the mean ELCC estimates that are obtained from our approximation are statistically significantly different with and without price uncertainty. We are unable to reject the null hypothesis at the 1% confidence, which suggests the ELCC estimates that are produced by our approximation are robust to price uncertainty.

TABLE IV
MEAN AND STANDARD ERROR (IN PARENTHESES) ELCC OF ENERGY STORAGE (% OF NAMEPLATE NET DISCHARGING CAPACITY) IN EXAMPLE FROM SECTION V-B USING APPROXIMATION

	$\bar{V}$		
$\bar{E}$	0	1000	9000
100	30 (0.01)	85 (0.00)	85 (0.00)
200	59 (0.00)	97 (0.00)	98 (0.00)
400	78 (0.25)	99 (0.00)	99 (0.01)
800	100 (0.00)	100 (0.00)	100 (0.00)

C. Case 3: Frequency Regulation

Case 3 includes frequency regulation, which changes operations compared to if energy storage conducts energy shifting only. In the latter case, energy-storage SOE varies between its extremes [10]. Providing frequency regulation requires having SOE away from its bounds, to have headroom to follow real-time frequency-regulation deployments [4], [23], [27].

Fig. 2 shows for one sample path of random variables hourly expected energy prices and expected SOE of energy storage with $\bar{E} = 200$ without and with frequency-regulation provision if $\bar{V} = 0$. Without frequency regulation, energy-storage SOE reaches a maximum of 200 MWh during hours 8–15 and a minimum of 0 MWh during hours 17–24 (*i.e.*, following the day's low- and high-price hours, respectively). Hours 15 and 16 have the highest energy prices of the day, and the expected SOE goes from 200 MWh to 0 MWh during these hours to exploit the high prices. If providing frequency regulation, energy-storage SOE is 200 MWh during hours 11–13 only and goes to 0 MWh during the course of hours 13–20.

Table V summarizes Case-3 ELCC estimates for the same sample path of the random variables that is summarized in Fig. 2. Comparing the ELCCs with $\bar{V} = 0$ that are in Table V to those that are in Tables II–IV shows the capacity-value impact of frequency-regulation provision. The differences stem from energy-storage SOE being at its maximum for fewer hours with frequency regulation, thereby reducing energy storage's ability to mitigate a loss of load. Having $\bar{V} > 0$ provides a financial incentive to maintain higher energy-storage SOE during high-LOLP hours, thereby increasing the energy-storage ELCC. For instance, hours 13–19 of the day that is shown in Fig. 2 have over 99% of the day's total LOLE. With $\bar{V} = 0$ and frequency-regulation provision, the average

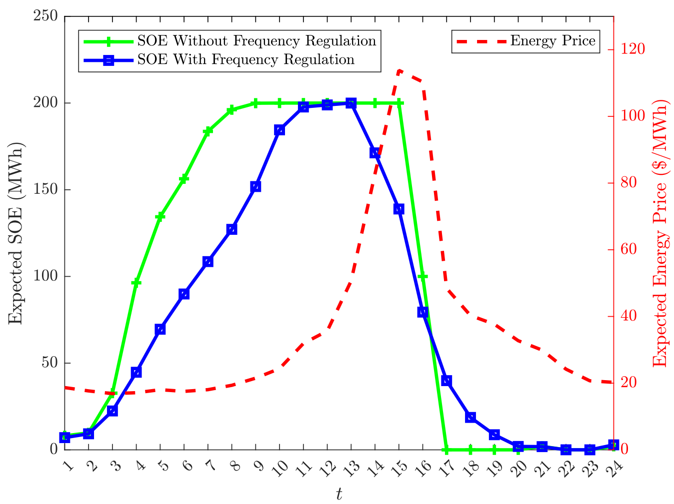

Fig. 2. Hourly expected SOE of energy storage without and with frequency-regulation provision and expected energy prices in example from Sections V-B and V-C with $\bar{E} = 200$ and $\bar{V} = 0$.

SOE of energy storage with $\bar{E} = 200$ during these hours is 93 MWh. Having $\bar{V} = 9000$ increases the average SOE during these hours to 153 MWh.

TABLE V
ELCC OF ENERGY STORAGE (% OF NAMEPLATE NET DISCHARGING CAPACITY) IN EXAMPLE FROM SECTION V-C USING APPROXIMATION

	$\bar{V}$		
$\bar{E}$	0	1000	9000
100	5	77	83
200	10	94	98
400	17	100	100
800	32	100	100

We conclude the analysis of the example by comparing expected energy-storage profit, as is computed in Line 15 of Algorithm 1, for the cases that are considered in Sections V-B and V-C. Table VI reports profits for the random-variable sample path that is summarized in Fig. 2. Increasing the value of $\bar{V}$ decreases energy-storage profit, through two effects. First, a higher value of $\bar{V}$ means that energy storage incurs higher non-performance penalties. Indeed, if $\bar{E} = 100$, non-performance penalties outweigh energy-storage profit from providing energy or frequency regulation. This result follows from the ELCCs that are reported in Tables IV and V being significantly lower than 100% if $\bar{E} = 100$. Second, a higher value of $\bar{V}$ incentivizes energy storage to maintain a higher SOE during high-LOLP hours, which reduces profit due to foregone energy and frequency-regulation revenue. Ultimately, energy storage should determine its optimal provision of capacity by weighing capacity payments against non-performance penalties. Such a comparison is beyond the scope of our work.

VI. CASE STUDY

This section expands upon Section V by simulating the operation and resultant ELCC of energy storage during the 31 days of the year with the highest daily peak LOLPs.

TABLE VI
EXPECTED ENERGY-STORAGE PROFIT ($ THOUSAND) IN EXAMPLE FROM SECTIONS V-B AND V-C USING APPROXIMATION

	Section V-B $\bar{V}$			Section V-C $\bar{V}$		
$\bar{E}$	0	1000	9000	0	1000	9000
100	9.4	-9.0	-97.6	23.7	-0.1	-68.2
200	18.2	9.2	-4.1	30.0	22.3	4.7
400	27.1	25.6	22.5	34.8	34.4	33.9
800	32.7	32.7	32.7	34.9	34.8	34.8

Examining days with high LOLPs is a reasonable approach to simplify an annual ELCC calculation, because a resource's ELCC is driven strongly by its ability to produce energy during a small subset of hours during the year with non-trivially high LOLPs [10], [46]–[48].

Table VII summarizes energy-storage ELCCs for the case study and shows similar trends to those that are observed in Section V. Energy-storage ELCC increases with $\bar{E}$ and $\bar{V}$. The former is due to energy-storage having more energy-storage capacity and the latter due to energy-storage SOE being managed more conservatively *vis-à-vis* high-LOLP hours. Different ELCCs that are reported in Tables V and VII, especially for cases with $\bar{V} = 0$, stem largely from different load and LOLP patterns between the example and case study. The example focuses on the single highest-LOLP day of the year. This day has a total LOLE (without energy storage) of 0.70. Moreover, there are five consecutive hours (hours 14–18) that account for 99.28% of this total LOLE. Thus, the ELCC of energy storage is connected closely to its ability to provide energy during these consecutive hours. By considering more days, the case study captures the ability of energy storage to supply energy during other high-LOLP hours. Overall, Tables V and VII illustrate an important tradeoff in ELCC modeling. If the model horizon is too short, ELCC estimates may misrepresent the ability of a resource to mitigate potential loss of load. Conversely, increasing the model horizon makes the computations more expensive.

TABLE VII
ELCC OF ENERGY STORAGE (% OF NAMEPLATE NET DISCHARGING CAPACITY) IN CASE STUDY FROM SECTION VI USING APPROXIMATION

	$\bar{V}$		
$\bar{E}$	0	1000	9000
100	5	70	88
200	16	92	97
400	43	99	100
800	69	100	100

Table VIII summarizes expected energy-storage profit during the 31 days that we model for the case study. The table shows qualitatively similar trends to those that are observed from Table VI. Increasing $\bar{V}$ decreases energy-storage profit, both due to non-performance penalties and because energy storage is more conservative in providing energy shifting and frequency regulation. The profit of energy storage increases with $\bar{E}$, due to its increased energy-storage capacity reducing the impact of potential non-performance penalties.

TABLE VIII
EXPECTED ENERGY-STORAGE PROFIT ($ THOUSAND) IN CASE STUDY FROM SECTION VI USING APPROXIMATION

	$\bar{V}$		
$\bar{E}$	0	1000	9000
100	640	547	252
200	780	752	683
400	896	892	887
800	989	989	989

VII. CONCLUSIONS

This paper examines the problem of assessing the resource-adequacy contribution of energy storage that provides multiple services, including energy shifting and frequency regulation. The key technical challenge that we address is capturing the complicated and uncertain SOE dynamics that providing frequency regulation entails. We propose a computationally intractable exact model and a three-step approximation method. The approximation method consists of (i) computing optimal decision policies from a discretized stochastic dynamic model, (ii) using the optimal decision policies in a rolling-horizon mixed-integer linear optimization, and (iii) Monte Carlo simulation.

We apply our model to a comprehensive case study that is based on a real-world electricity system. In doing so, we find a tradeoff between using energy storage to provide capacity, energy shifting, and frequency regulation. Maximizing capacity value requires maintaining a high SOE, whereas frequency regulation calls for maintaining headroom between the SOE and its bounds. As such, without properly designed market signals (or other incentives), the capacity value of energy storage that provides frequency regulation can decrease by as much as 68 percentage points compared to if it provides energy shifting only. Thus, our model lends itself to many potential uses *vis-à-vis* examining the resource-adequacy contribution of energy storage. Energy-storage owners can use our model to determine how to use their assets between these competing services. Electricity-system planners can use our model to capture energy storage in resource-adequacy assessments. Finally, our model can provide insights to market designers regarding how capacity auctions or mechanisms that include energy storage as capacity resources should be structured to maximize energy-storage value towards that application.

Our model represents all decisions and state dynamics at hourly time steps. In practice, most frequency-regulation markets require resources to follow a dispatch signal with an approximately four-second time resolution [49], [50]. In addition, many markets connect frequency-regulation payments to the ability of a resource to follow the real-time dispatch signal [51]. We do not model the four-second dynamics of the frequency-regulation signal, because we assume that the energy-storage has the operational and ramping flexibility to follow the signal. Rather, our model is formulated to ensure that there is sufficient headroom between the SOE and its bounds to allow the requiste energy-storage charging and discharging to follow the aggregate hourly signal. We do not believe that the four-second dynamics of the frequency-regulation signal would have any significant impact on our model results. Nonetheless, extending our model to capture these dynamics would be a natural topic for future study.

ACKNOWLEDGMENT

The authors thank the editors, four anonymous reviewers, and A. Sorooshian for suggestions and comments.

REFERENCES

[1] "EPRI-DOE Handbook for Energy Storage for Transmission and Distribution Applications," Electric Power Research Institute and the U.S. Department of Energy, Palo Alto, CA and Washington, DC, USA, Tech. Rep. 1001834, 2003.

[2] R. Sioshansi, P. Denholm, and T. Jenkin, "Market and Policy Barriers to Deployment of Energy Storage," *Economics of Energy & Environmental Policy*, vol. 1, pp. 47–63, March 2012.

[3] P. Saugier, A. Atayi, T. Hinchliffe, N. Marinho, and P. Loevenbruck, "Exploring multi-services business cases for a storage unit in various grid schemes," in *CIGRE Session 2018*. Paris, France: Conseil International des Grands Réseaux Électriques, 26-31 August 2018.

[4] X. Xi, R. Sioshansi, and V. Marano, "A Stochastic Dynamic Programming Model for Co-optimization of Distributed Energy Storage," *Energy Systems*, vol. 5, pp. 475–505, September 2014.

[5] G. Strbac, M. Aunedi, I. Konstantelos, R. Moreira, F. Teng, R. Moreno, D. Pudjianto, A. Laguna, and P. Papadopoulos, "Opportunities for Energy Storage: Assessing Whole-System Economic Benefits of Energy Storage in Future Electricity Systems," *IEEE Power and Energy Magazine*, vol. 15, pp. 32–41, September-October 2017.

[6] L. L. Garver, "Effective Load Carrying Capability of Generating Units," *IEEE Transactions on Power Apparatus and Systems*, vol. PAS-85, pp. 910–919, August 1966.

[7] R. Billinton and R. N. Allan, *Reliability Evaluation of Power Systems*. Boston, Massachusetts: Pitman Advanced Publishing Program, 1984.

[8] K. Yagi, R. Sioshansi, and P. Denholm, "Evaluating a Concentrating Solar Power Plant as an Extended-Duration Peaking Resource Solar Energy," *Solar Energy*, vol. 191, pp. 686–696, October 2019.

[9] ——, "Using Concentrating-Solar-Power Plants as Economic Carbon-Free Capacity Resources," *Energy Conversion and Management: X*, vol. 12, p. 100112, December 2021.

[10] R. Sioshansi, S. H. Madaeni, and P. Denholm, "A Dynamic Programming Approach to Estimate the Capacity Value of Energy Storage," *IEEE Transactions on Power Systems*, vol. 29, pp. 395–403, January 2014.

[11] P. Denholm and T. Mai, "Timescales of Energy Storage Needed for Reducing Renewable Energy Curtailment," National Renewable Energy Laboratory, Golden, CO, Tech. Rep. NREL/TP-6A20-68960, September 2017.

[12] G. Edwards, S. Sheehy, C. J. Dent, and M. C. M. Troffaes, "Assessing the contribution of nightly rechargeable grid-scale storage to generation capacity adequacy," *Sustainable Energy, Grids and Networks*, vol. 12, pp. 69–81, December 2017.

[13] H. Kim, R. Sioshansi, E. Lannoye, and E. Ela, "A Stochastic-Dynamic-Optimization Approach to Estimating the Capacity Value of Energy Storage," *IEEE Transactions on Power Systems*, vol. 37, pp. 1809–1819, May 2022.

[14] M. A. Mansouri and R. Sioshansi, "The Effect of Natural-Gas Prices on Power-System Reliability," *Current Sustainable/Renewable Energy Reports*, vol. 8, pp. 164–173, September 2021.

[15] B. Klöckl and G. Papaefthymiou, "An effort to overcome the chronological modeling methods for energy storage devices," in *2005 International Conference on Future Power Systems*. Amsterdam, Netherlands: Institute of Electrical and Electronics Engineers, 18 November 2005.

[16] P. Hu, R. Karki, and R. Billinton, "Reliability evaluation of generating systems containing wind power and energy storage," *IET Generation, Transmission & Distribution*, vol. 3, pp. 783–791, August 2009.

[17] L. H. Koh, G. Z. Yong, W. Peng, and K. J. Tseng, "Impact of Energy Storage and Variability of PV on Power System Reliability," *Energy Procedia*, vol. 33, pp. 302–310, 2013.

[18] Y. Zhou, P. Mancarella, and J. Mutale, "Framework for capacity credit assessment of electrical energy storage and demand response," *IET Generation, Transmission & Distribution*, vol. 10, pp. 2267–2276, 9 June 2016.

[19] I. Konstantelos, P. Djapic, G. Strbac, P. Papadopoulos, and A. Laguna, "Contribution of energy storage and demand-side response to security of distribution networks," *CIRED - Open Access Proceedings Journal*, vol. 2017, pp. 1650–1654, October 2017.

[20] B. J. Kirby, "Frequency Regulation Basics and Trends," Oak Ridge National Laboratory, Tech. Rep. ORNL/TM-2004-291, December 2004.

[21] M. Kintner-Meyer, "Regulatory Policy and Markets for Energy Storage in North America," *Proceedings of the IEEE*, vol. 102, pp. 1065–1072, July 2014.

[22] Y. Sun, T. Levin, J. Kwon, Q. Xu, N. Singhal, E. Ela, Z. Zhou, C. Crespo Montanes, B. Frew, R. B. Hytowitz, A. D. Mills, M. Heidarifar, P. de Mello, A. Botterud, and B. F. Hobbs, "Research Priorities and Opportunities in United States Competitive Wholesale Electricity Markets," National Renewable Energy Laboratory, Golden, CO, Tech. Rep. NREL/TP-A20-77521, May 2021.

[23] M. A. Mansouri and R. Sioshansi, "Comparing Electric Water Heaters and Batteries as Energy-Storage Resources for Energy Shifting and Frequency Regulation," *IEEE Open Access Journal of Power and Energy*, vol. 10, pp. 164–175, 4 January 2023.

[24] R. H. Byrne and C. A. Silva-Monroy, "Estimating the Maximum Potential Revenue for Grid Connected Electricity Storage: Arbitrage and Regulation," Sandia National Laboratories, Albuquerque, NM, Tech. Rep. SAND2012-3863, December 2012.

[25] K. Anderson and A. El Gamal, "Co-optimizing the value of storage in energy and regulation service markets," *Energy Systems*, vol. 8, pp. 369–387, May 2017.

[26] J. H. Kim, F. Kahrl, A. D. Mills, R. Wiser, C. Crespo Montañés, and W. Gorman, "Variable Renewable Energy Participation in U.S. Ancillary Services Markets: Economic Evaluation and Key Issues," in *IEEE 49th Photovoltaics Specialists Conference*. Philadelphia, PA: Institute of Electrical and Electronics Engineers, 5-10 June 2022.

[27] X. Xi and R. Sioshansi, "A Dynamic Programming Model of Energy Storage and Transformer Deployments to Relieve Distribution Constraints," *Computational Management Science*, vol. 13, pp. 119–146, January 2016.

[28] B. Cheng and W. B. Powell, "Co-Optimizing Battery Storage for the Frequency Regulation and Energy Arbitrage Using Multi-Scale Dynamic Programming," *IEEE Transactions on Smart Grid*, vol. 9, pp. 1997–2005, May 2018.

[29] A. Berrada, K. Loudiyi, and I. Zorkani, "Valuation of energy storage in energy and regulation markets," *Energy*, vol. 115 Part 1, pp. 1109–1118, 15 November 2016.

[30] N. Yu and B. Foggo, "Stochastic valuation of energy storage in wholesale power markets," *Energy Economics*, vol. 64, pp. 177–185, May 2017.

[31] Y. G. Rebours, D. S. Kirschen, M. Trotignon, and S. Rossignol, "A Survey of Frequency and Voltage Control Ancillary Services—Part II: Economic Features," *IEEE Transactions on Power Systems*, vol. 22, pp. 358–366, February 2007.

[32] Z. Zhou, T. Levin, and G. Conzelmann, "Survey of U.S. Ancillary Services Markets," Argonne National Laboratory, Lemont, IL, Tech. Rep. ANL/ESD-16/1 Rev1, June 2016.

[33] *PJM Manual 18: PJM Capacity Market*, 47th ed., PJM Interconnection, L.L.C., 27 January 2021.

[34] R. Sioshansi and A. J. Conejo, *Optimization in Engineering: Models and Algorithms*, ser. Springer Optimization and Its Applications. Gewerbestraße 11, 6330 Cham, Switzerland: Springer Nature, 2017, vol. 120.

[35] W. Kempton and J. Tomić, "Vehicle-to-grid power fundamentals: Calculating capacity and net revenue," *Journal of Power Sources*, vol. 144, pp. 268–279, 1 June 2005.

[36] R. Sioshansi, P. Denholm, J. Arteaga, S. Awara, S. Bhattacharjee, A. Botterud, W. Cole, A. Cortés, A. de Queiroz, J. DeCarolis, Z. Ding, N. DiOrio, Y. Dvorkin, U. Helman, J. X. Johnson, I. Konstantelos, T. Mai, H. Pandžić, D. Sodano, G. Stephen, A. Svoboda, H. Zareipour, and Z. Zhang, "Energy-Storage Modeling: State-of-the-Art and Future Research Directions," *IEEE Transactions on Power Systems*, vol. 37, pp. 860–875, March 2022.

[37] H. Kim, R. Sioshansi, and A. J. Conejo, "Benefits of Stochastic Optimization for Scheduling Energy Storage in Wholesale Electricity Markets," *Journal of Modern Power Systems and Clean Energy*, vol. 9, pp. 181–189, January 2021.

[38] Y. Fang, Z. Qu, J. Zhang, H. Xu, and G. L. Qi, "Simultaneous charging and discharging performance for a latent thermal energy storage system with a microencapsulated phase change material," *Applied Energy*, vol. 275, p. 115353, 1 October 2020.

[39] F. Wu and R. Sioshansi, "A Stochastic Operational Model for Controlling Electric Vehicle Charging to Provide Frequency Regulation," *Transportation Research Part D: Transport and Environment*, vol. 67, pp. 475–490, February 2019.

[40] W. B. Powell, *Approximate Dynamic Programming: Solving the Curses of Dimensionality*. Hoboken, New Jersey: Wiley-Interscience, 2007.

[41] T. W. Anderson and D. A. Darling, "A Test of Goodness of Fit," *Journal of the American Statistical Association*, vol. 49, pp. 765–769, 1954.

[42] A. C. Davison and D. V. Hinkley, *Bootstrap Methods and their Application*, ser. Cambridge Series in Statistical and Probabilistic Mathematics. Cambridge, United Kingdom: Cambridge University Press, 1997.

[43] G. Cavaliere, H. B. Nielsen, and A. Rahbek, "An Introduction to Bootstrap Theory in Time Series Econometrics," in *Oxford Research Encyclopedia of Economics and Finance*, J. H. Hamilton, Ed. Oxford, United Kingdom: Oxford University Press, January 2021.

[44] R. J. Hyndman and G. Athanasopoulos, *Forecasting: Principles and Practice*, 3rd ed. Melbourne, Australia: Otexts, 31 May 2021.

[45] A. Carpinone, M. Giorgio, R. Langella, and A. Testa, "Markov chain modeling for very-short-term wind power forecasting," *Electric Power Systems Research*, vol. 122, pp. 152–158, May 2015.

[46] S. H. Madaeni, R. Sioshansi, and P. Denholm, "Comparing Capacity Value Estimation Techniques for Photovoltaic Solar Power," *IEEE Journal of Photovoltaics*, vol. 3, pp. 407–415, January 2013.

[47] D. Gami, R. Sioshansi, and P. Denholm, "Data Challenges in Estimating the Capacity Value of Solar Photovoltaics," *IEEE Journal of Photovoltaics*, vol. 7, pp. 1065–1073, July 2017.

[48] P. Denholm, J. Nunemaker, P. Gagnon, and W. Cole, "The potential for battery energy storage to provide peaking capacity in the United States," *Renewable Energy*, vol. 151, pp. 1269–1277, May 2020.

[49] U. Helman, B. F. Hobbs, and R. P. O'Neill, "The Design of US Wholesale Energy and Ancillary Service Auction Markets: Theory and Practice," in *Competitive Electricity Markets: Design, Implementation, Performance*, F. P. Sioshansi, Ed. Elsevier, 2008, pp. 179–243.

[50] E. Ela, V. Gevorgian, A. Tuohy, B. Kirby, M. Milligan, and M. O'Malley, "Market Designs for the Primary Frequency Response Ancillary Service—Part I: Motivation and Design," *IEEE Transactions on Power Systems*, vol. 29, pp. 421–431, January 2014.

[51] B. Xu, Y. Shi, D. S. Kirschen, and B. Zhang, "Optimal Battery Participation in Frequency Regulation Markets," *IEEE Transactions on Power Systems*, vol. 33, pp. 6715–6725, November 2018.

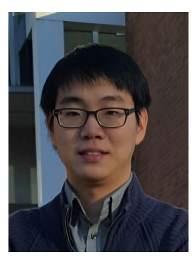

Hyeong Jun Kim (S'16) received his B.S. degree in industrial and management engineering from Hanyang University, Ansan, gyeonggi-do, South Korea, and an M.S. and Ph.D. in industrial and systems engineering from The Ohio State University, Columbus, OH, USA.

His research interests are in optimization, energy storage, energy-market analysis, and game theory.

Ramteen Sioshansi (M'11–SM'12–F'21) holds the B.A. degree in economics and applied mathematics and the M.S. and Ph.D. degrees in industrial engineering and operations research from University of California, Berkeley, Berkeley, CA, USA and an M.Sc. in econometrics and mathematical economics from London School of Economics and Political Science, London, U.K.

He is a professor in Department of Engineering and Public Policy and Department of Electrical and Computer Engineering, Director of Carnegie Mellon Electricity Industry Center, and a faculty affiliate of Wilton E. Scott Institute for Energy Innovation at Carnegie Mellon University, Pittsburgh, PA, USA and an adjunct professor in Department of Integrated Systems Engineering at The Ohio State University, Columbus, OH, USA. His research focuses on analyzing renewable and sustainable energy systems and the design of restructured competitive electricity markets.

Eamonn Lannoye (M'09) received B.E. and Ph.D. degrees from University College Dublin, Dublin, Ireland and an MBA from Imperial College London, London, U.K.

He works as Senior Project Manager at EPRI Europe where his interests include grid reliability, transmission-system operation, and the interface between transmission-system and distribution-system operators.

Erik Ela (M'06–SM'15) received the B.S.E.E. degree from Binghamton University, Binghamton, NY, USA, the M.S. degree from Illinois Institute of Technology, Chicago, IL, USA, and the Ph.D. degree from University College Dublin, Dublin, Ireland.

He is currently a Principal Technical Leader at Electric Power Research Institute. He has held positions at National Renewable Energy Laboratory and New York Independent System Operator. His research interests include power-system operations, electricity-market design, power-system planning, and reliability services.